A composite 3D seismic velocity model for Utah FORGE

Finger, C.[1], Niemz, P.[2], Ermert, L.[3], Lanza, F.[3]

[1] Fraunhofer IEG, Fraunhofer Research Institution for Energy Infrastructure and Geothermal Systems, Bochum, Germany

[2] University of Utah, Salt Lake City, Utah, USA

[3] ETH Zürich, Zurich, Switzerland

Corresponding authors:

P. Niemz: pniemz.seismology@gmail.com

C. Finger: claudia.finger@ieg.fraunhofer.de

1. PREFACE

We invite you to use this model, improve it, and update it, and we encourage you to share your new velocity model so all researchers working on Utah FORGE can use it.

2. Introduction

The Utah FORGE project is located in central Utah (USA), close to the town of Milford, UT. The Mineral Mountains, located directly to the east of the Utah FORGE site, constitute the eastern border of the Milford Valley. From a regional perspective, the location is part of the easternmost Basin-and-Range extensional regime, close to the transition to the stable Colorado Plateau. However, the adjacent Mineral Mountains are of Quarternary volcanic origin: The mountain range and valley are not a horst-and-graben structure.

The Mineral Mountains batholith (granitoid and metamorphic rocks) is thought to have tilted during the core complex formation, resulting in a westward dipping basement boundary beneath the valley (Coleman and Walker, 1994) (Fig. 1b). The basement boundary constitutes a sharp impedance contrast between the granitoid/metamorphic rocks (S phase velocity V_s >3000 m/s) and the basin filling (V_s <2500 m/s).

The local coordinate reference at Utah FORGE is the wellhead of the injection borehole 16A(78)-32 at 1650 m elevation at 38.50402147N, 112.8963897W (blue cross in Fig. 1a). The corresponding UTM coordinates (UTM Zone N12 NAD83(2011), EPSG:6341) are: East 334641.1891 and North 4263443.693.

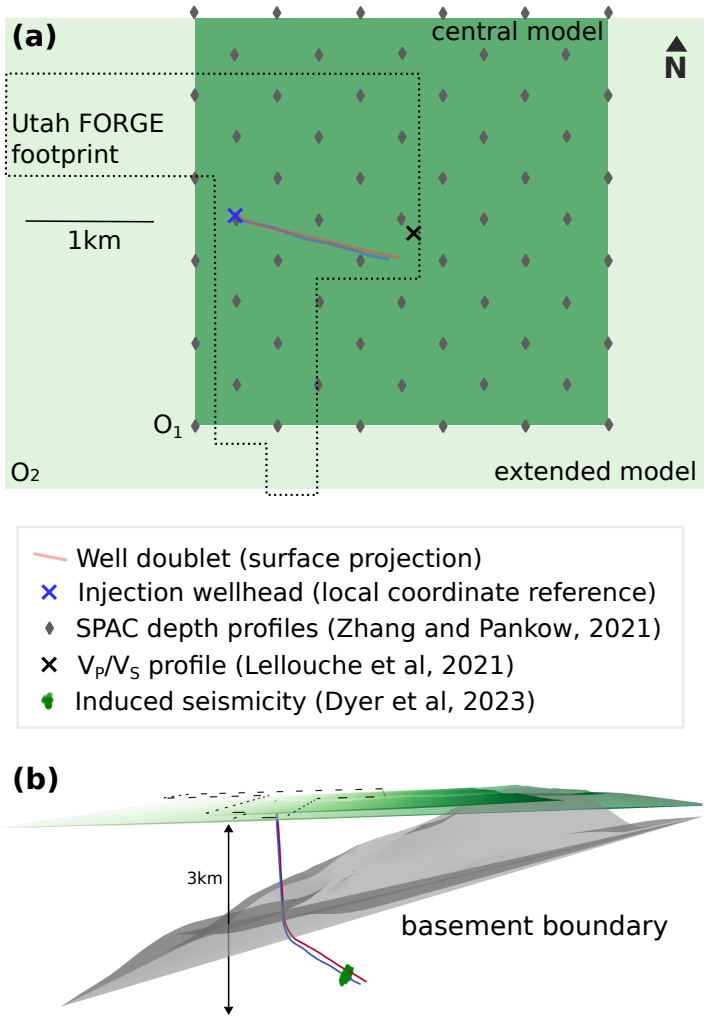

Figure 1: *The composite 3D velocity model for Utah FORGE combines the quasi-3D shear velocity model from Zhang and Pankow (2021) with a V_p/V_s profile form a central borehole (78-32, marked by a black cross in a) and the basement boundary mapped via reflection seismics (b). For the calibration of the model, we rely on induced microseismic events in the geothermal reservoir at a depth of approx. 2.5 km. The local station distribution requires an extension of the model (see Fig. 3). A blue cross marks the wellhead of the injection well (16A(78)-32) which is the reference of the local coordinate system.*

For the composite 3D seismic velocity model for P and S phases (V_p and V_s), we compiled information from several local studies regarding seismic velocities and structural information. The quasi 3D velocity from Zhang and Pankow (2021) is the base for our model. Grey diamonds mark the locations of 61 V_s depth profiles provided in their study in Fig. 1a. The base model is enriched by (1) vp/vs ratios from (Lellouch et al., 2021) obtained from the injection well (blue cross and blue line in Fig. 1a and b), (2) shallow-depth velocity estimates from Zhang et al. (2019), (3) a reflection seismic survey mapping the sediment-basement boundary (Fig. 1, Miller et al. (2019); Podgorney (2018)) and (4) deep basement velocity obtained from downhole monitoring (pers. comm. B. Dyer).

The model was calibrated based on the seismic activity induced during the stimulations in April 2022 (Moore et al., 2023). This activity was monitored by surface and downhole networks. The downhole catalog of Dyer et al. (2023a) is used as a reference. The two surface networks, (1) the temporary nodal array (Whidden et al., 2023) and (2) the regional permanent seismic network of the University of Utah Seismograph Stations (University of Utah, 1962, UUSS), are used for the model calibration. We compare observed arrivals of P and S phases from the surface networks to theoretical arrivals calculated based on the high-quality locations of the downhole catalog and the 3D velocity model.

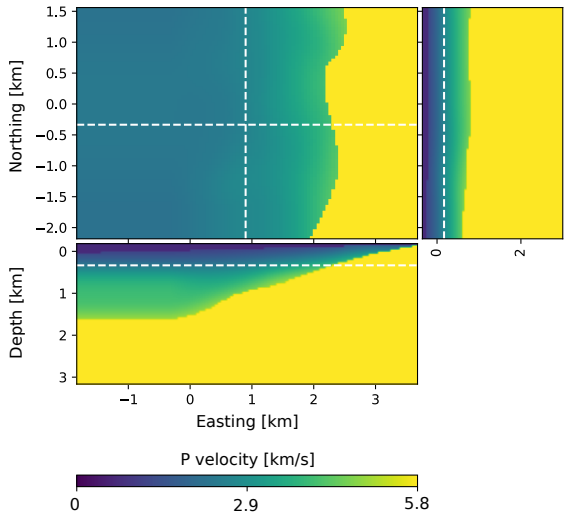

Figure 2: *Map view (depth of 250m) and depth sections for the extended composite 3D velocity model for Utah FORGE. White dashed lines mark the profiles.*

3. Contributing studies and data sets

Combining information from different studies helps to overcome the limitations of single data sets, e.g., due to limited depth resolution, and provides a ready-to-use 3D velocity model for P and S phases. The data sets used to set up the composite model are described below.

3.1. Base model

Our composite model is predominately based on the quasi-3D velocity model of Zhang and Pankow (2021). Their SPAC (spatial auto-correlation) shear wave velocity model provides 61 1D S-wave velocity profiles distributed over an area of approximately 3 km by 3 km. The model reflects sub-horizontal velocity layers in the basin and the westward dipping basement layer. The model has the best resolution between a depth of 30 m and 2000 m and was obtained by fitting within a frequency range of 0.2 to 5 Hz. See Zhang and Pankow (2021) for further details on the methods used.

3.2. Near-surface shear wave velocity

The upper approximately 30 m of the shear-wave velocity model derived via SPAC are not well resolved (Zhang and Pankow, 2021), so we replace those values with an approximate vs30 velocity of 400m/s as reported in Zhang et al. (2019) for the Utah FORGE site.

3.3. Vp and Vs in the basement

To overcome the limited depth resolution of the SPAC model and to enhance the impedance contrast we fix the velocities below the basement boundary to V_p = 5800 m/s and V_s =3400 m/s. These velocities were estimated via the travel time of P and S waves excited by perforation shots and recorded by downhole geophones during the 2022 stimulation at Utah FORGE (Moore et al., 2023). The locations of the perforation shots are well-known, so the seismic velocities could be estimated by assuming straight ray paths in a homogeneous medium. The estimated velocities require only negligible station corrections (-0.0005 to -0.002 s) for the downhole geophones (Dyer et al., 2023b, B. Dyer, pers. comm.), which shows that they are very good approximations for the velocities in the source volume activated by the high-pressure injections.

Both velocities are rounded to the closest 100 m/s, since the uncertainty of the velocity estimates reflected in the station corrections is higher than the original precision would imply.

3.4. Vp/Vs ratios

Lellouch et al. (2021) provide V_p and V_s velocity profiles for Utah FORGE well 78-32 (Fig. 1a) based on the seismic arrivals from perforation shots along distributed acoustic sensing (DAS) cable. The V_s profile of Lellouch et al. (2021) coincides well with the V_s profile closest to well 78-32 from Zhang and Pankow (2021). We use the velocity profiles of Lellouch et al. (2021) to get an approximate V_p/V_s profile for the basin filling.

4. Velocity model setup

The velocity model was set up using a single *python* script provided with this data set. The main steps of the velocity model setup are described below:

[1] We adjust each 1D S phase velocity profile from Zhang and Pankow (2021) for the elevation of the used geophone node by shifting them to the according depth in a predefined depth range from -200 to 3100 m relative to the local reference elevation. A negative depth corresponds to an elevation above the reference height.

[2] Subsequently, we set the first 30m below the surface to 400 m/s for each profile. For the provided 3D model we extend this low-velocity layer up to -200m to ensure that receivers are within a rock layer in the model. However, we provide an option (*add_vacuum_layer*) to set profile points above the surface to a very low velocity of 10 m/s to simulate the sharp contrast of the free surface.

[3] The lower end of each profile up to the sediment-basement boundary is fixed at 3400 m/s, corresponding to the downhole homogeneous model.

[4] Under the assumption that all sedimentary layers are present across the basin while having different thicknesses, we stretch or compress the depth of the V_p/V_s ratio profile from Lellouch et al. (2021) above the basement boundary to fit the basin depth. V_p/V_s below the basement boundary was set to 1.71 to

match the constant V_p of 5800 m/s.

[5] We interpolate linearly between the refined, elevation-adjusted 1D velocity profiles of P and S velocities to obtain a regularly-spaced 3D grid of S velocities with a spacing of 50m extending from -200 to 3100 m in depth, from -312 to 2938 m in E-W direction, and from -1623 to 1577 m in N-S direction (O_1 and central model in Fig. 1).

[6] We smooth the velocity with a Gaussian filter. The standard deviation for the Gaussian kernel was set to 5 grid points. Finally, we reset the velocity below the basement boundary to the fixed velocities for P and S.

[7] The extension of the grid beyond the area covered by the base model was achieved by appending the last slice of the model for the given direction until filling the extended model space. The extension is required to include stations located farther away (Fig. 1a and 3). As before, we fixed the velocities below the basement boundary in the extended volumes to 3400 m/s and 5800 m/s. The origin of the extended model (O_2, Fig. 1) is at -1811 m, -2128 m. The extension of the model is only implemented for the NLL output of the grid.

[8] The 3D model can be exported as a big-endian binary file, in netCDF format, and in NonLinLoc's (NLL) 3D velocity model format (Lomax et al., 2000, 2009). The first two provide velocities while the latter is formatted to be directly used in the location routines of NLL (SLOW_LEN, $1/V_p$ * grid_spacing). Information on the grid origin, grid spacing, and the number of grid nodes is included in the headers of the NLL and netCDF files.

[9] For the big-endian binary file, we calculate the density from V_p using the empirical relation from Brocher (2005) to provide all necessary parameters for the simulation of elastic seismic wave propagation.

5. Model calibration

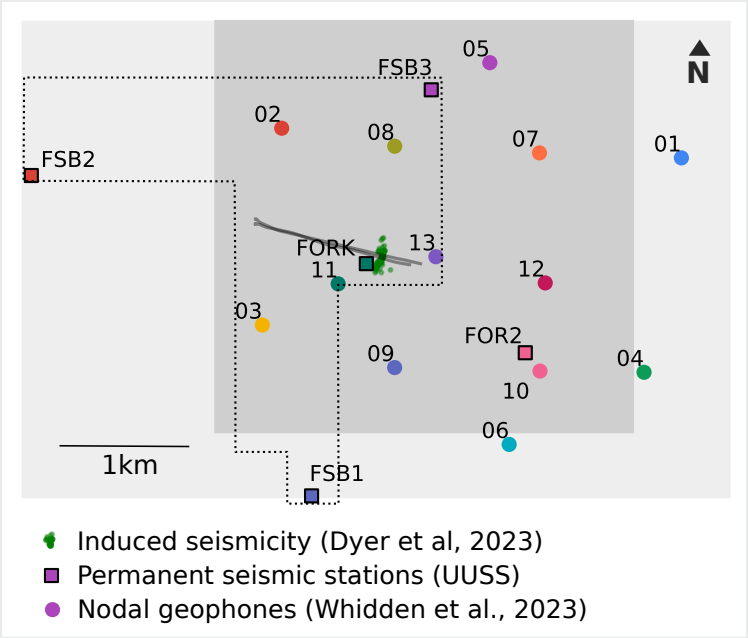

Figure 3: *Station distribution relative to the central model (dark grey area) and the extended model (light grey). The extension of the central model is required to include volumes with additional stations, particularly for the UUSS permanent network.*

The 3D velocity model was calibrated and tested by comparing P and S arrival picks with theoretical arrival times for induced microseismic events during stage 3 of the 2022 stimulation experiment at Utah FORGE (Moore et al., 2023). The theoretical travel times were calculated using NonLinLoc and high-quality event locations of the downhole catalog (Dyer et al., 2023a,b). Picking was done manually on the stacked traces of 13 nodal geophone patches (Whidden et al., 2023) and on 5 permanent network stations of the UUSS (Fig.3). In Fig. 4, we also show the theoretical arrival times when obtained from the local velocity model used by UUSS for the authoritative seismic catalog (Tab. 1). The differences between travel times from the 1D and the 3D velocity model reveal the importance of considering the dipping basement boundary for local relocations. The best fit between the given manual picks and theoretical arrivals was achieved with a standard deviation of 5 grid nodes for the Gaussian smoothing kernel. We tested standard deviations between 1 and 10. The overall fit between the observed and the theoretical arrivals calculated from the model is very good. Most P and S arrivals do not deviate by more than 10% (Fig. 4). The depth

velocity profile from the 3D model closest to the well for which Lellouch et al. (2021) obtained P and S wave velocities shows a good fit (Fig. 5). See section 6 for a discussion on deviations between observed and theoretical travel times (e.g., FSB3 (purple) and FSB1 (blue) of the permanent UUSS network or 01 (blue) and 06 (light blue) of the temporary deployment).

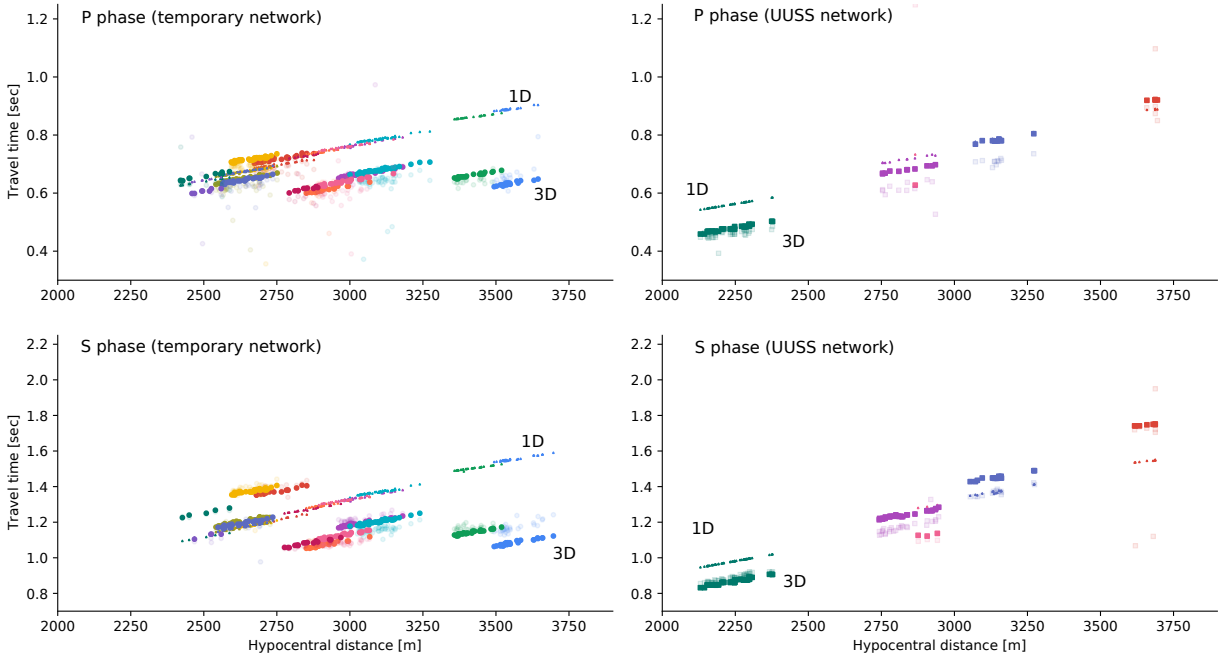

Figure 4: *Comparison of manual phase picks (transparent circles) and theoretical arrival times for the composite 3D model (circles) and the 1D model (triangles)*

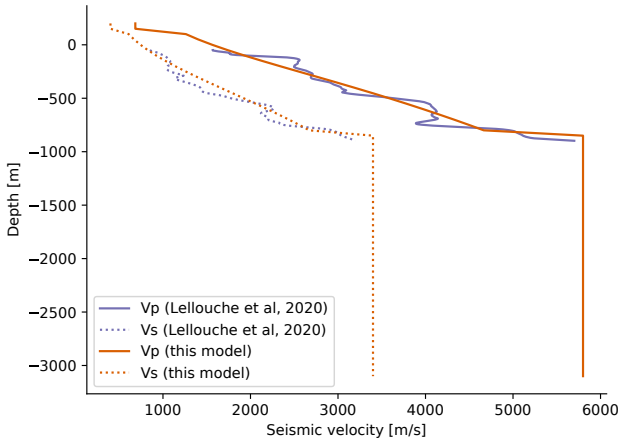

Figure 5: *Comparison of the P and S velocity profiles in well 78A-32 (Lellouch et al., 2021) and the closest depth profile extracted from our 3D model.*

Table 1: *1D velocity model used for locations in the UUSS authoritative seismic catalog in the area of Utah FORGE based on Bjarnason and Pechmann (1989). The layer depth was adjusted to the reference elevation of the local coordinate system. The model is given in nd format (Crotwell et al., 1999)*

Depth [km]	V_p [km/s]	V_s [km/s]
-0.200	3.400	1.950
1.690	3.400	1.950
1.690	5.900	3.390
17.25	5.900	3.390
17.25	6.400	3.680
28.15	6.400	3.680
28.15	7.500	4.310
42.15	7.500	4.310
42.15	7.900	4.540

6. Known Issues/Shortcomings

The simple linear extension of the SPAC model beyond its boundaries is bound to errors. That becomes most apparent for FSB1 and 01. Both are far outside of the area covered by the SPAC model. 01 is closer to the Mineral Mountains, where the basement rock crops out. The model is too fast for 01 because it is mainly based on topography and the basement boundary, which probably leads to an underestimation of the sediment layer thickness. FSB1 shows no improvement compared to the 1D velocity model. A topographic low in the sediment-basement boundary, as seen in the reflection seismic survey, might have led to deviations in the basin sedimentation, thus altering the velocity distribution in this area. The same might apply to 06.

The user of this velocity model should be aware that this model might not be suitable for their particular study, e.g. due to different frequency contents of their signal. The calibration was done for microseismic events with dominant frequencies between 20 and 40 Hz.

7. Resources

The data of the base model from Zhang and Pankow (2021) (61 profiles and a location file) are available via the Geothermal Data Repository (GDR) (`https://dx.doi.org/10.15121/1776592`). The velocity profile from Lellouch et al. (2021) can be downloaded from the author's GitHub repository (`https://github.com/ariellellouch/FORGE/tree/master/Vel_DAS.txt`). The basement boundary provided by Podgorney

(2018) is also available at the GDR (`https://dx.doi.org/10.15121/1495398`, `https://gdr.openei.org/files/1107/top_granitoid_vertices.csv`). To rerun the Python script for setting up the velocity model, the user has to download the data sets mentioned above and set the correct local file paths pointing to them.

The script requires the following packages:

- numpy
- scipy
- matplotlib
- utm
- nllgrid (if using the NonLinLoc grid output)
- xarray (if using the NetCDF grid output)

REMARK: At the time of the publication of this model, the pip package of nllgrid was not up-to-date. Please refer to the package's GitHub repository (`https://github.com/claudiodsf/nllgrid`) and follow the instructions for an installation via GitHub.

To read the big-endian binary file into python for modification, the user can use the following options, with *dimz*, *dimx*, and *dimy* being the number of gridpoints in each direction, in the memmap function of the numpy package:

```
numpy.memmap([your_filename],dtype='>f4',mode='r',shape=(dimz,dimx,dimy,3),order='F')
```

References

I. T. Bjarnason and J. C. Pechmann. Contemporary tectonics of the Wasatch front region, Utah, from earthquake focal mechanisms. *Bulletin of the Seismological Society of America*, 79(3):731–755, 06 1989. doi:10.1785/BSSA0790030731.

T. M. Brocher. Empirical relations between elastic wavespeeds and density in the Earth's crust. *Bulletin of the Seismological Society of America*, 95(6):2081–2092, 2005. doi:10.1785/0120050077.

D. S. Coleman and J. D. Walker. Modes of tilting during extensional core complex development. *Science*, 263(5144):215–218, 1994.

H. P. Crotwell, T. J. Owens, and J. Ritsema. The TauP Toolkit: Flexible Seismic Travel-time and Ray-path Utilities. *Seismological Research Letters*, 70(2):154–160, 03 1999. doi:10.1785/gssrl.70.2.154.

B. Dyer, D. Karvounis, and F. Bethmann. Microseismic event catalogues from the well 16A(78)-32 stimulation in April, 2022 in Utah FORGE., 2023a. Data set retrieved from `https:\doi.org/10.31905/52CC4QZB`.

B. C. Dyer, F. Bethmann, D. Karvounis, P. Meier, K. L. Pankow, P. Wannamaker, J. Moore, J. Rutledge, and A. Ammon. Innovative Microseismic Monitoring Tools and Configurations for Geothermal Applications. In *Proceedings of the World Geothermal Congress*, Beijing, China, Sept. 2023b.

A. Lellouch, N. J. Lindsey, W. L. Ellsworth, and B. L. Biondi. Comparison between Distributed Acoustic Sensing and Geophones: Downhole Microseismic Monitoring of the FORGE Geothermal Experiment. *Seismological Research Letters*, 91(6):3256–3268, 2021. doi:10.1785/0220200149.

A. Lomax, J. Virieux, P. Volant, and C. Berge-Thierry. Probabilistic Earthquake Location in 3D and Layered Models. In C. H. Thurber and N. Rabinowitz, editors, *Advances in Seismic Event Location*, Modern Approaches in Geophysics, pages 101–134. Springer Netherlands, Dordrecht, 2000. doi:10.1007/978-94-015-9536-0_5.

A. Lomax, A. Michelini, and A. Curtis. Earthquake Location, Direct, Global-Search Methods. In R. A. Meyers, editor, *Encyclopedia of Complexity and Systems Science*, pages 1–33. Springer, New York, NY, 2009. doi:10.1007/978-3-642-27737-5_150-2.

J. Miller, R. Allis, and C. Hardwick. Interpretation of Seismic Reflection Surveys Near the FORGE Enhanced Geothermal Systems Site, Utah. In R. Allis and J. N. Moore, editors, *Geothermal Characteristics*

of the Roosevelt Hot Springs System and Adjacent FORGE EGS Site, Milford, Utah, volume 169 of *Utah Geological Survey Miscellaneous Publication*. Utah Geological Survey, Sept. 2019. doi:10.34191/MP-169-H.

J. Moore, J. McLennan, K. Pankow, A. Finnila, B. Dyer, D. Karvounis, F. Bethmann, R. Podgorney, J. Rutledge, P. Meir, P. Xing, C. Jones, B. Barker, S. Simmons, and B. Damjanac. Current activities at the Utah frontier observatory for research in geothermal energy (FORGE): A laboratory for characterizing, creating and sustaining enhanced geothermal systems. In *Proceedings 51st US Rock Mechanics/Geomechanics Symposium*, pages ARMA–2023–0749, 2023. doi:10.56952/ARMA-2023-0749.

R. Podgorney. Utah FORGE: Earth Model Mesh Data for Selected Surfaces, 2018. Data retrieved from `https://gdr.openei.org/submissions/1107`.

University of Utah. University of utah regional seismic network, 1962.

K. Whidden, G. M. Petersen, and K. L. Pankow. Seismic Monitoring of the 2022 Utah FORGE Stimulation: The View from the Surface. In *PROCEEDINGS*, pages SGP –TR–224, 2023.

H. Zhang and L. K. Pankow. High-resolution Bayesian spatial autocorrelation (SPAC) quasi-3-D *Vs* model of Utah FORGE site with a dense geophone array. *Geophysical Journal International*, 225(3):1605–1615, 2021. doi:10.1093/gji/ggab049. Data set retrieved from `https://dx.doi.org/10.15121/1776592`.

H. Zhang, K. Pankow, and W. Stephenson. A Bayesian Monte Carlo inversion of spatial auto-correlation (SPAC) for near-surface Vs structure applied to both broad-band and geophone data. *Geophysical Journal International*, 217(3):2056–2070, June 2019. doi:10.1093/gji/ggz136.